



**HAL**  
open science

## Three-Dimensional Structure and Dynamics of African Easterly Waves. Part II: Dynamical Modes

Nicholas M. J. Hall, George M. Kiladis, Chris D. Thorncroft

► **To cite this version:**

Nicholas M. J. Hall, George M. Kiladis, Chris D. Thorncroft. Three-Dimensional Structure and Dynamics of African Easterly Waves. Part II: Dynamical Modes. *Journal of the Atmospheric Sciences*, 2006, 63 (9), pp.2231 à 2245. 10.1175/JAS3742.1 . insu-00385795

**HAL Id: insu-00385795**

**<https://insu.hal.science/insu-00385795>**

Submitted on 11 Mar 2021

**HAL** is a multi-disciplinary open access archive for the deposit and dissemination of scientific research documents, whether they are published or not. The documents may come from teaching and research institutions in France or abroad, or from public or private research centers.

L'archive ouverte pluridisciplinaire **HAL**, est destinée au dépôt et à la diffusion de documents scientifiques de niveau recherche, publiés ou non, émanant des établissements d'enseignement et de recherche français ou étrangers, des laboratoires publics ou privés.

## Three-Dimensional Structure and Dynamics of African Easterly Waves. Part II: Dynamical Modes

NICHOLAS M. J. HALL

*Laboratoire d'étude des Transferts en Hydrologie et Environnement, Grenoble, France*

GEORGE N. KILADIS

*Earth System Research Laboratory, NOAA, Boulder, Colorado*

CHRIS D. THORNCROFT

*Department of Earth and Atmospheric Sciences, University at Albany, State University of New York, Albany, New York*

(Manuscript received 6 June 2005, in final form 18 November 2005)

### ABSTRACT

A primitive equation model is used to study the linear normal modes of the African easterly jet (AEJ). Reanalysis data from the summertime mean (June–September; JJAS) flow is used to provide zonally uniform and wavy basic states. The structure and growth rates of modes that grow over West Africa on these basic states are analyzed. For zonally uniform basic states, the modes resemble African easterly waves (AEWs) as in many previous studies, but they are quite baroclinic and surface intensified.

For wavy basic states the modes have a longitudinal structure determined by the AEJ. They have a surface-intensified baroclinic structure upstream and a deep barotropic structure downstream, as confirmed by energy conversion diagnostics. These modes look remarkably similar to the composite easterly wave structures found by the authors in a companion paper. The similarity extends to the phase relationship of vertical velocity with streamfunction, which resembles OLR composites, suggesting a dynamical influence on convection.

Without damping, the mode for the wavy basic state has a growth rate of  $0.253 \text{ day}^{-1}$ . With a reasonable amount of low-level damping this mode is neutralized. It has a period of 5.5 days and a wavelength of about 3500 km. Further results with monthly mean basic states show slight variations, as the wave packet essentially follows displacements of the jet core. Experiments focused on specific active and passive years for easterly waves (1988 and 1990) do not yield significantly different results for the modes. These results, and in particular, the stability of the system, lead to the conclusion that barotropic–baroclinic instability alone cannot explain the initiation and intermittence of AEWs, and a finite-amplitude initial perturbation is required.

### 1. Introduction

It has long been assumed that African easterly waves (AEWs) result from a mixed barotropic–baroclinic instability of the African easterly jet (AEJ). This understanding is derived from two observed phenomena. First, the time mean latitude–height structure of the summertime midtropospheric wind over West Africa is consistent with dynamical instability for a zonal flow. Second, the waves themselves have a composite struc-

ture consistent with the extraction of energy from both the horizontal and vertical shear of the AEJ. The latter is clearly seen in the diagnostics presented in the companion paper Kiladis et al. (2006, hereafter Part I). In this paper we use a dynamical model to find the preferred modal structures associated with the observed zonally varying AEJ, and compare them with the composites in Part I. We will then reexamine the stability of the AEJ.

The idea that easterly waves result from an instability was first put forward by Burpee (1972) who noted a midtropospheric reversal in meridional potential vorticity gradient at the latitude of the AEJ. A more comprehensive climatology of reversals in potential vortic-

---

*Corresponding author address:* Dr. Nicholas M. J. Hall, LTHE, BP53, 38041 Grenoble CEDEX 9, France.  
E-mail: Nick.Hall@hmg.inpg.fr

TABLE 1. Details from previous idealized studies of AEWs.

	Basic state	$U_{\max}$ ( $\text{m s}^{-1}$ )	Growth rate ( $\text{day}^{-1}$ )	Period (days)	Wavelength (km)	Phase speed ( $\text{m s}^{-1}$ )
Rennick (1976)	Enhanced jet (originally based on August 1957–64, 5E)	22.6	0.37	2.2	3000	15.8
Simmons (1977)	Idealized, based on GATE*	15	0.27	5	3900	9
Mass (1979)	“Typical” jet core construct based on the last week of August 1963	16.5	0.26	3.86	2500	7.5
Kwon (1989)	Idealized analytic fit to GATE*	17.7	0.28–0.31	3.74	3100	9.6
Chang (1993)	Northern flank analytic neutral profile	$\frac{\partial\theta}{\partial y} = 0.7$	2	3–5	2000–2750	9–6
Thorncroft and Hoskins (1994a)	Idealized, based on GATE*	15	0.28	4.8	3500	8.4
Thorncroft and Hoskins (1994b)	Initially as in TH94a	13 at day 6	0.16 at day 6	—	—	—
Paradis et al. (1995)	Idealized from ECMWF composites averaged over a wavelength	15	0.4–0.5	4.9–5.3	3300	
Thorncroft (1995)	Enhanced equatorward shear, reduced poleward static stability	15	0.37	4.5	3000	7.8
Grist et al. (2002)	NCEP data for wet and dry years (10°W–20°E)	10 (wet) 12 (dry)	0.42–0.88 (wet) 0.25–0.35 (dry)	—	3000	—

\* Reed et al. (1977): Their profile is based on 10°E–30°W with  $U_{\max} = 13 \text{ m s}^{-1}$ .

ity gradient is presented by Dickinson and Molinari (2000) showing extensive regions (20°E–30°W) where the gradient changes sign. In these regions the potential vorticity gradient combined with the low-level temperature gradient satisfies the Charney–Stern (1962) and Fjortoft (1950) necessary conditions for instability over a range of longitudes. These conditions refer to a zonal flow, and one of the questions we will address in this paper is how appropriate stability calculations based on zonally uniform flow profiles are for the three-dimensional AEJ. There have been many examples of such calculations, and they have shown steadily increasing sophistication and realism. These idealized studies include the work of Rennick (1976), Simmons (1977), Mass (1979), Kwon (1989), Miller and Lindzen (1992), Chang (1993), Thorncroft and Hoskins (1994a,b, hereafter TH94a,b), Paradis et al. (1995), Thorncroft (1995), and recently Grist et al. (2002) who are the first to actually use observed zonal winds as a basic state for linear normal mode studies of the AEJ. The paper by Paradis et al. contains a particularly good summary of most of this work, but here in Table 1 we repeat some of the essential features of the basic states used and the results in terms of growth rates and wave properties.

Note that all of the studies cited above use a zonally uniform basic state, and with the exception of TH94b and Thorncroft (1995) they are all linear. They simulate wave structures that grow on a steady zonal flow and various choices have been made about which longitude,

or range of longitudes, best represents the aggregate experience of a wave as it passes through the AEJ (see Table 1). Little can be deduced from these studies about longitudinal variations in wave structure and amplitude, except where these variations result from nonlinear downstream development. It is clear from Part I, and from previous work with more limited datasets (most notably in the energetic analysis of Norquist et al. 1977), that there are considerable variations in wave structure from the wave inception region around 20°E to the dissipation region in the mid-Atlantic. As the waves grow over the land surface they are characterized by sloping or bowed trough lines and baroclinic conversions, extracting energy from the basic-state vertical shear (latent heat release in convection is also a possible source of eddy energy). As they leave the coast they become more barotropic, and extract energy from the basic-state horizontal shear. Similar characteristics have also been noted in diagnostics from GCMs (see, e.g., Céron and Guérémy 1999; Fyfe 1999). Does this behavior depend on nonlinear development (as in TH94b; Thorncroft 1995) or can we explain it in a linear framework in terms of the interaction of the wave with a longitudinally varying AEJ?

In this paper we address this question for the first time. We build on the work of Thorncroft and collaborators (in fact we use a variant of the same model) but instead of an idealized zonally uniform basic state we use fully three-dimensional time-averaged National

Centers for Environmental Prediction–National Center for Atmospheric Research (NCEP–NCAR) reanalyzed fields taken from the summers (June–September; JJAS) of 1968–99. Three-dimensional normal mode structures are calculated and compared with the wave characteristics presented in Part I. The growth rates and wave structures are compared with more traditional experiments based on observed zonal flows. The sensitivity of these modes to a simple representation of surface drag and heat exchange is also investigated in the same spirit as Hall and Sardeshmukh (1998) in their study of the midlatitude jets. In the light of these results, previously accepted wisdom on the stability of the AEJ and thus the origin of AEWs will be reexamined.

The novel features of this work are thus as follows: a consideration of the zonally varying nature of the AEJ and its effect on the dynamical modes; the inclusion of more realistic aspects of the zonal mean circulation, including surface westerlies and the mean meridional circulation; a comparison of the results with the observations presented in Part I; and an investigation of the sensitivity of these results to a simple prescription of surface damping, with a discussion of the consequences of our findings. In section 2, the model, the basic states, and the techniques of normal mode extraction are presented. Results with zonally uniform basic states are then shown in section 3 and with zonally varying (wavy) basic states in section 4. Discussion and interpretation is then offered in section 5 and conclusions in section 6.

## 2. Methods, parameters, and experiments

### a. Normal mode calculations

The model used in this study is essentially the same as the one used by Simmons (1977) and by Thorncroft and collaborators. It is a global spectral primitive equation model, used here with a horizontal resolution of T31 and 10 equally spaced sigma levels. A semi-implicit 22.5-min time step is used to integrate the full nonlinear equations for vorticity, divergence, temperature, and log (surface pressure). The only physical parameterization in the basic runs is the 12 h  $\nabla^6$  diffusion of momentum and temperature. Normal modes of a given basic state are calculated following the method used by Hall and Sardeshmukh (1998, hereafter HS98).

In general, a basic state taken from observations will not be a solution of the primitive equations, so if it is used as an initial condition in the model there will be some development,

$$\frac{d\mathbf{X}}{dt} = \text{PE}(\mathbf{X}) \neq 0, \quad (1)$$

where  $\mathbf{X}$  is a state vector that represents the instantaneous state of the model and is set to the initial condition  $\mathbf{X}_0$  at  $t = 0$ .  $\text{PE}(\mathbf{X})$  is a nonlinear operator that defines the action of the primitive equations plus whatever diffusion or damping we choose to include. We now add a forcing term to the right-hand side of (1) defined as  $-\text{PE}(\mathbf{X}_0)$ . This is calculated by integrating (1) for one time step. The forcing term  $-\text{PE}(\mathbf{X}_0)$  represents the maintenance of the basic state by diabatic forcing and transient eddies combined. The use of this forcing is a departure from the balanced idealized experiments seen in most previous studies. It means that the eddy modal structures deduced as a property of the basic-state  $\mathbf{X}_0$  are not independent of the effect of eddies on  $\mathbf{X}_0$ . However,  $\mathbf{X}_0$  represents a more realistic depiction of the AEJ that is more relevant for the growth of disturbances. More detailed justifications for proceeding with such a calculation are given in HS98. Having added the term  $-\text{PE}(\mathbf{X}_0)$  to (1), we now add a small random perturbation  $\mathbf{X}'$  to the initial condition and integrate. The following equation will be satisfied:

$$\frac{d\mathbf{X}'}{dt} = \text{LPE}_{\mathbf{X}_0}(\mathbf{X}') + O(\mathbf{X}'^2), \quad (2)$$

which is linear provided  $\mathbf{X}'$  remains small.  $\text{LPE}_{\mathbf{X}_0}$  is the linearization of  $\text{PE}$  about the basic state  $\mathbf{X}_0$ . If  $\mathbf{X}'$  is forced to remain small by repeated rescaling, a long integration of (2) will eventually yield a single structure that satisfies the eigenvalue relation

$$\text{LPE}_{\mathbf{X}_0}(\mathbf{X}_e) = (\sigma + i\omega)\mathbf{X}_e. \quad (3)$$

The mode grows at rate  $\sigma$  and oscillates with angular frequency  $\omega$ . For three-dimensional basic states  $\text{LPE}_{\mathbf{X}_0}$  is generally asymmetric so  $\mathbf{X}_e$  is complex, and two real spatial structures are needed to define the mode. The time development of the real perturbation  $\mathbf{X}'$  can thus be written

$$\mathbf{X}'(\mathbf{x}, t) = [\mathbf{X}_A(\mathbf{x}) \sin\omega t + \mathbf{X}_B(\mathbf{x}) \cos\omega t]e^{\sigma t}. \quad (4)$$

We will refer to the structures  $\mathbf{X}_A$  and  $\mathbf{X}_B$  as the A and B phases of the mode, which cycles from A to B to  $-A$  to  $-B$  and back to A. An integration of 1000 days is ample to isolate the fastest-growing structure. In cases where  $\sigma$  is negative, the system is stable and the first eigenmode of (3) is the slowest-decaying structure. The technique remains the same, but  $\mathbf{X}'$  must be repeatedly scaled up instead of down.

The dominant growing modes for the global circulation consist of wave trains in the midlatitude storm track regions. To make sure that the emerging mode is relevant to AEWs further modifications of the PE op-

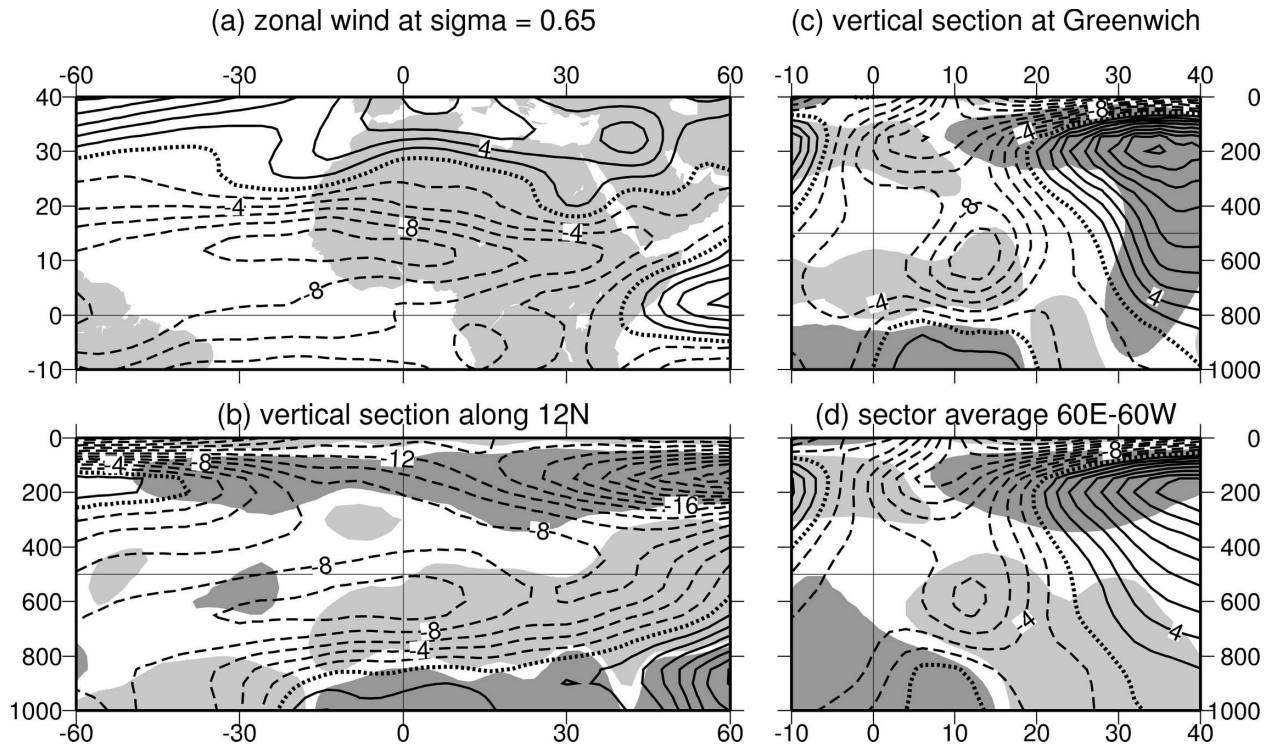


FIG. 1. Summertime (JJAS) zonal wind over West Africa from NCEP reanalyses 1968–98 (a) at  $\sigma = 0.65$ , (b) vertical latitudinal section at  $12^{\circ}\text{N}$ , (c) vertical meridional section at  $0^{\circ}$ , (d) vertical meridional sector average from  $60^{\circ}\text{W}$  to  $60^{\circ}\text{E}$ . Contours are every  $2\text{ m s}^{-1}$ , zero contour dotted, negative contours dashed. Shading shows where the associated meridional wind exceeds  $0.5\text{ m s}^{-1}$ . Heavy shading denotes southerlies, light shading northerlies. Southerlies near the surface reach maxima of about (c)  $7\text{ m s}^{-1}$  and (d)  $3.5\text{ m s}^{-1}$  south of the equator. At  $12^{\circ}\text{N}$  at the  $0^{\circ}$  meridian, this value is about  $4\text{ m s}^{-1}$ .

erator are necessary. The experiments shown in this paper have an extra damping on momentum outside the rectangular region from  $60^{\circ}\text{W}$  to  $60^{\circ}\text{E}$  and  $1.9^{\circ}\text{S}$  to  $31.5^{\circ}\text{N}$ . For experiments with zonally uniform basic states, the damping is a function of latitude only, so the waves grow in an undamped channel. The damping is carried out on the  $96 \times 48$  Gaussian grid at all levels with a time scale of one day except on the boundary grid points where the time scale is two days. It has no physical meaning and serves merely to keep the solution close to the basic state outside the West African region and allow perturbations to develop inside the region.

In some experiments a surface-intensified linear damping is also applied to the emerging African easterly wave modes. It is intended as a simple representation of turbulent transfer of momentum and heat with the surface. The average damping rates used here give time scales of two days for momentum and four days for temperature near the surface (the coefficient actually decreases linearly from the surface to  $\sigma = 0.8$ ). In the free atmosphere (above  $\sigma = 0.8$ ) time scales for momentum and temperature are 30 and 10 days. This level of damping is actually quite conservative com-

pared to the range of values that could be considered realistic, and is only half the intensity needed to stabilize the midlatitude winter jets (see HS98). It is also similar to the damping rate used by TH94a, but unlike them, we will find that it has a significant stabilizing effect on the easterly wave modes.

#### b. The basic states

Daily NCEP reanalysis data (Kalnay et al. 1996) has been spectrally analyzed at T31 and interpolated to give vorticity, divergence, and temperature on 10 equally spaced sigma levels. Orography is not represented in the model so the surface pressure seen by the model is actually calculated from the 1000-mb geopotential height and 1000-mb temperature. A time–height-independent divergence correction has been applied as outlined by Hall (2000).

Figure 1 shows the zonal wind over West Africa in the summertime. This June–September mean for 1968–98 will provide the basic state for most of the experiments. The AEJ is situated at  $12^{\circ}\text{N}$  at about 600 mb, with maximum intensity on the Greenwich meridian. The first thing to note is that the reanalyzed jet is weak compared to the jet maxima typically chosen for this

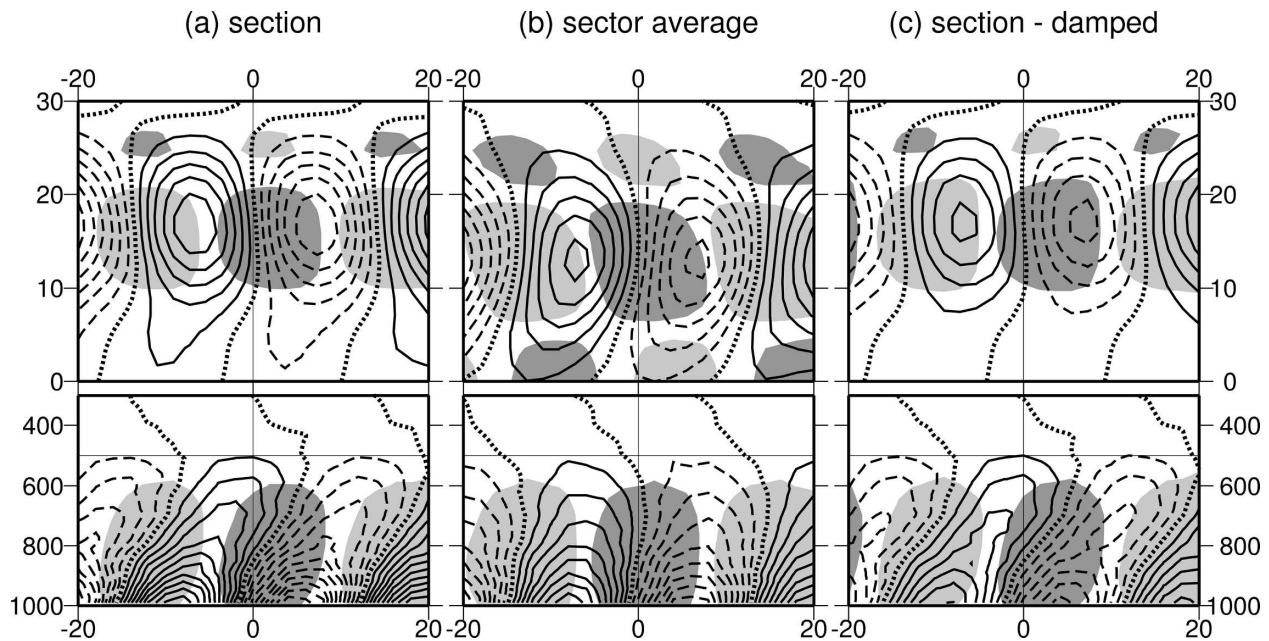


FIG. 2. Normal mode structures from zonally uniform basic states. Undamped modes for (a) Greenwich section and (b) sector average 60°W–60°E, and (c) damped mode for Greenwich section. Horizontal streamfunction is shown at  $\sigma = 0.85$  in upper panels and in a vertical section along 15°N in lower panels. Vertical velocity is also indicated by heavy shading (ascent) and light shading (descent). Contour intervals are arbitrary but consistent between different projections, zero contour dotted, negative contours dashed.

type of study shown in Table 1. While the Global Atmospheric Research Program (GARP) Atlantic Tropical Experiment (GATE) composite (Reed et al. 1977) has a maximum of  $13 \text{ m s}^{-1}$  and many previous studies use  $15 \text{ m s}^{-1}$  and up, the maximum easterlies in Fig. 1 are  $10 \text{ m s}^{-1}$ . This is consistent with the basic states used by Grist et al. (2002) who also use NCEP data. This alone might be expected to impinge upon the modal growth rates. TH94b find a halving of linear growth rates associated with a reduction of jet speed from  $15$  to  $13 \text{ m s}^{-1}$  in the first six days of a nonlinear integration. Grist et al. show a very wide range of growth rates for their different composites.

Perhaps part of the reason for the different jet speeds chosen in previous studies is that in addition to variations in observed peak jet amplitude, further uncertainty comes from the choice of a representative longitude for a given observed flow. Peak values of  $10 \text{ m s}^{-1}$  extend over about 40 degrees of longitude, so easterly waves may interact with weaker zonal flows for part of their lifetime. We will study the two contrasting basic states shown in Fig. 1, representing a peak jet and a spatially averaged jet, respectively the meridional section at Greenwich with a  $10 \text{ m s}^{-1}$  jet core, and the zonal mean from 60°W to 60°E with an  $8 \text{ m s}^{-1}$  jet core. The zonal mean meridional wind present in these sections is indicated by shading. Experiments with zonally uniform basic states based on these sections will be

compared with experiments based on the full three-dimensional flow.

The summertime mean flow is a convenient point of departure. The AEJ does of course vary both intraseasonally and interannually. Results from individual months will also be shown to give an idea how this variability affects the modes, and a more comprehensive account of the relationship between AEJ intensity and easterly wave activity will be given in a following contribution.

### 3. Zonally uniform basic states

Before presenting new results for basic states with a zonally varying jet structure, in this section we show some results with zonally uniform basic states to provide some continuity with previous work. Figure 2 shows the horizontal and vertical structure of the streamfunction and vertical velocity for the fastest-growing modes that develop on the Greenwich section and the 60°W–60°E mean basic states shown in Fig. 1. Some statistics of the wave properties are given in Table 2. For the Greenwich section basic state, the wave is situated on the poleward flank of the AEJ and is fairly symmetrical about a zonal axis, with a wavelength of about 3000 km, similar to many previous studies (see Table 1), and slightly smaller than in observations (Part I). Upward motion occurs in the northerlies,

TABLE 2. Normal mode wave properties for a selection of experiments on the JJAS 1968–98 climatological basic state. The last two columns show energy conversion diagnostics [see Eq. (5)]. The fifth column shows the relative magnitudes of the four terms in the denominator. The last column shows the full ratio expressed in (5) for the entire wave structure, and in the case of wavy basic states, for three zonal sectors: 60°–30°W, 30°W–0°, and 0°–30°E.

Basic state	Growth rate (day <sup>-1</sup> )	Period (days)	Wavelength (km)	Phase speed (m s <sup>-1</sup> )	Denominator Eq. (5) term 1:2:3:4	Full Eq. (5)
Greenwich section	0.473	4.88	29.80	7.07	11:62:13:13	2.16
60°W–60°E sector avg	0.144	5.44	29.80	6.34	7:83:0:9	0.45
Damped Greenwich	0.272	5.56	29.70	6.18	12:51:22:14	4.84
JJAS wavy basic state	0.253	5.80	2460–5155	4.91–10.29	7:71:-7:15	1.32:1.17/1.54/1.14
Damped JJAS wavy basic state	-0.003	5.51	3400–5620	7.14–11.81	14:61:-11:14	2.38:0.95/2.30/2.68

as it does at low levels in the experiments of TH94a and in the observed waves over the continent in Part I. The wave grows at a rate of 0.473 day<sup>-1</sup>, or an *e*-folding time scale of 2 days, which is relatively fast (see Table 1) despite the relatively weak jet. The vertical section shows a surface-intensified structure quite unlike that shown by TH94a, with most of the amplitude below the jet and phase lines tilting against the shear consistent with baroclinic growth both above and below the jet as shown by the reversal in slope of the zero contour at jet height. The lack of amplitude above the jet core compared to the observations in Part I may be due to the fact that the simulated modes are dry, whereas deep convection will be associated with substantial circulations above the jet. The growing structure is clearly baroclinic and grows on the near-surface temperature gradient, which is about twice as strong as in TH94a. Despite the weaker jet core in the reanalysis data, there is an intense low-level shear at this longitude owing to the presence of mean westerlies at the surface. These westerlies form an important part of the baroclinic signature of the basic state, which are not represented in more idealized studies [with the exceptions of Rennick (1976) and Kwon (1989)]. Reduced static stability com-

pared to idealized basic states also has the effect of intensifying the baroclinic growth and related enhanced surface amplitudes, as shown by Thorncroft (1995). Figure 3 shows some meridional fluxes associated with the wave structure, which are also surface intensified. As in Part I, there is southward temperature flux everywhere as expected below an easterly jet. This changes sign aloft but is extremely weak above the jet. At the jet level, westerly momentum flux is southward at the latitude of the wave, as observed (cf. Fig. 13 in Part I). Since the wave center is north of the jet center, this is consistent with a deceleration of the jet, or a barotropic wave growth.

The dominant baroclinic nature of the wave is reflected in the Lorenz energy conversion terms for the wave, which have been calculated following the definitions given in Norquist et al. (1977). Specifically we are interested in a measure of the relative importance of baroclinic and barotropic energy conversions to the growth of the wave. This is given by the ratio of baroclinic conversions from eddy available potential energy (AE) to eddy kinetic energy (KE) and barotropic conversions from zonal kinetic energy (KZ) to eddy kinetic energy, defined as

$$\frac{\text{AE} \rightarrow \text{KE}}{\text{KZ} \rightarrow \text{KE}} = \frac{R \int_0^{p_s} \{[\omega^* T^*]_p\} dp}{\int_0^{p_s} \{[u^* v^*]_y + [v^{*2}]_y + [u^* \omega^*]_p + [v^* \omega^*]_p\} dp}, \quad (5)$$

and is shown in Table 2 for various basic states. Square brackets denote zonal means over an entire wavelength or wave packet, \* denotes departures therefrom, curly brackets denote meridional mean, and subscripts denote derivatives. Note that the terms in the denominator involving  $[v]$  do not appear for experiments with idealized basic states with a purely zonal flow, but they do turn out to be quite important for our observed

zonal mean basic states, which include a zonal mean meridional wind. The second term in the denominator is actually larger than the first (see Table 2). Calculated in this way, the relative magnitudes of baroclinic (AE – KE) and barotropic (KZ – KE) contributions to the wave kinetic energy are 0.68 and 0.32; that is, a ratio of 2.16.

In summary, the diagnostics shown for the Green-

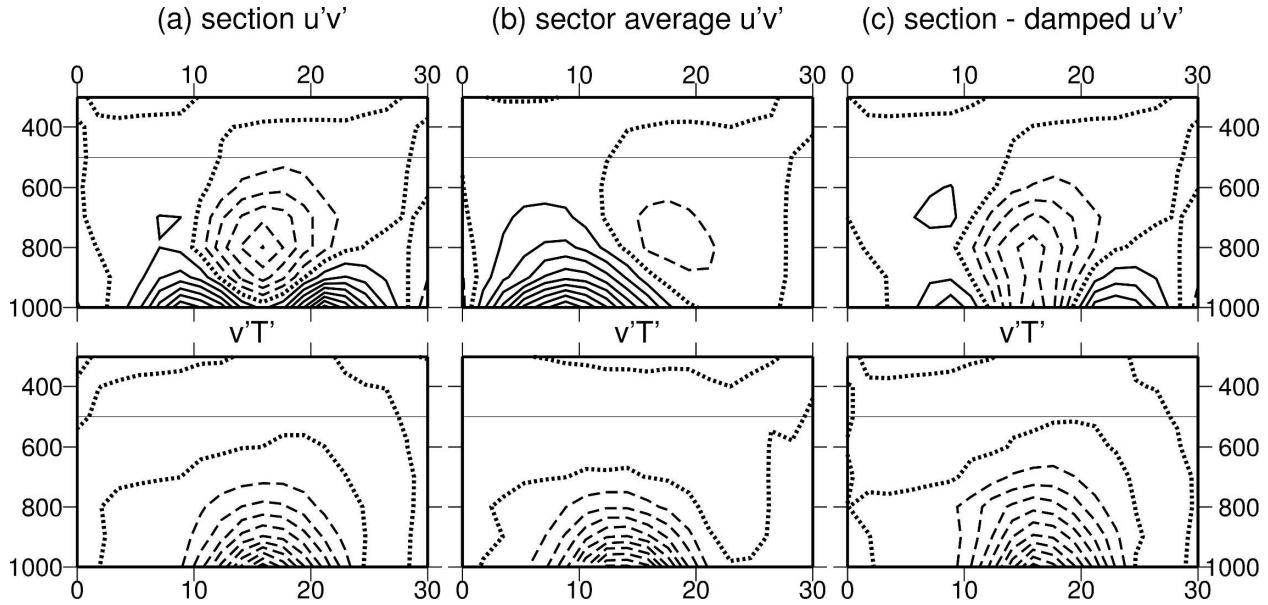


FIG. 3. Northward fluxes of (top) westerly momentum and (bottom) temperature associated with modal structures derived from zonally uniform basic states. (a) Greenwich section basic state, (b) sector average 60°W–60°E, (c) damped mode on Greenwich section basic state. Contour intervals are arbitrary, zero contour dotted, negative contours dashed.

wich section basic state show a growing easterly wave with a reasonable wavelength and phase speed, and all the indications of a mixed barotropic/baroclinic instability. Questions still arise about whether this is an appropriate basic state, and whether even with the relatively fast growth rate found for this basic state we can conclude that AEWs are generated primarily through the instability mechanism. Is a sufficient amplification of the wave possible as it passes through the jet region? Before commenting further on this we will consider results for other basic states.

The AEJ tracks from east to west at a constant latitude, so the jet core in the sector mean basic state is in the same position as for the Greenwich section. However, Fig. 2 shows that for this basic state the waves develop further south and now straddle the jet core. The wave appears to be somewhat less surface intensified and is less tilted against the low-level shear. The growth rate is greatly reduced, with an *e*-folding time of 7 days. The wavelength remains the same but the wave now propagates more slowly, consistent with the weaker jet. The importance of the southern flank of the wave is also seen in the northward flux of westerly momentum (Fig. 3) that now contributes to the barotropic growth, also reflected in the asymmetric tilt of the wave about the jet axis, as in the observations (see Part I, Figs. 3 and 4). Energy conversion diagnostics now show a very different signature, with barotropic conversions now outweighing baroclinic conversions by more than two to one. Thus despite some superficial similarities

between the modes growing on meridional section and sector mean basic states, we see some important differences in the balance of processes at work. It is difficult to decide which basic state best characterizes the growth of AEWs.

Before moving on to zonally varying basic states, we will examine the effect of low-level damping on these simpler modes. The last panel to the right in Fig. 2 shows the result of the Greenwich section experiment with added low-level damping. There is almost no change in the horizontal structure of the wave, but the surface intensification is abated (note that when interpreting these figures it must be remembered that the amplitudes are arbitrary and only the structure can be meaningfully compared from one experiment to another). The growth rate is almost halved and the phase speed is also slightly reduced. The structure of the associated fluxes (Fig. 3c) also remains similar except for a deeper structure in temperature flux, consistent with a weaker contribution at low levels. Despite this, the system is still very baroclinic in terms of energy conversions. Although the damping has weakened the low-level temperature flux, it has also reduced the velocity correlation terms. To be precise, the term involving gradients of zonal mean meridional wind mentioned above  $[v'^2][v]_y$  is relatively small and the cancelling effect of the correlation of vertical momentum flux with vertical shear  $[u^* \omega^*][u]_p$  has increased (details are shown in Table 2). These effects serve to keep the ratio of baroclinic-to-barotropic conversions high, as shown in the

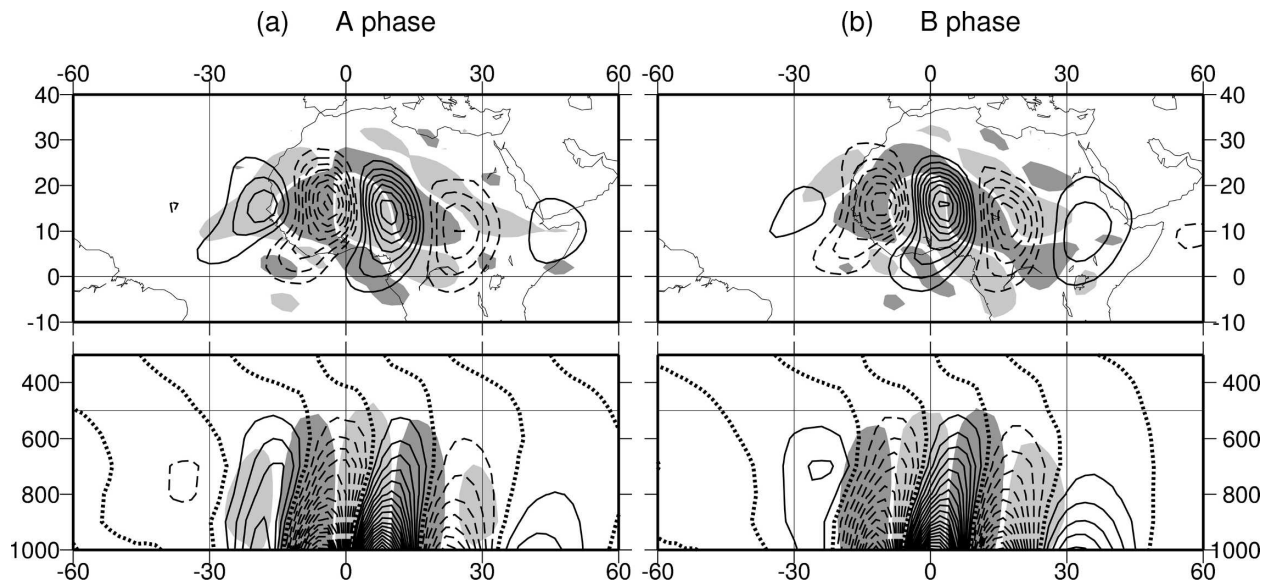


FIG. 4. Undamped modal structures for a wavy JJAS basic state. Horizontal streamfunction (contours) and vertical motion (shading) at (top)  $\sigma = 0.85$  and (bottom) vertical section at  $15^\circ\text{N}$ . Contour intervals are arbitrary but constant, negative contours dashed, zero contour dotted in vertical plots, omitted in horizontal plots. Ascent is heavily shaded and descent lightly shaded. Two quadrature phases are shown: (a) A phase, (b) B phase.

last column of Table 2. The effect of the term  $[v^{*2}]_y$  is completely absent in idealized studies where the basic state has no meridional flow, and we may wonder which is the more representative.

Finally the sector mean experiment was also repeated with low-level damping (not shown). For this basic state the damping stifles all growth and the emergent mode (the slowest decaying) is not of easterly wave form, but a large-scale standing oscillation. This does not mean that easterly waves are impossible for this combination of basic state and damping, just that they are not the slowest decaying mode. A relatively modest rate of low-level damping is thus seen to be capable of stabilizing the system, depending on the choice of basic state.

#### 4. Zonally varying basic states

The fastest-growing mode associated with the three-dimensional structure of the AEJ of Fig. 1 is shown in Fig. 4. The A and B phases are shown as explained in section 2. An isolated wave train emerges, approximately coincident with the strongest part of the jet, appearing over the horn of Africa and dissipating in the Atlantic. It has a similar wavelength and frequency to the sector-average mode described above (see Table 2). In fact the mode has a variable wavelength and phase speed, but a single frequency, so the wave decelerates and shortens as it arrives from the east. To obtain this

easterly wave solution, midlatitude modes were suppressed by damping outside the region as described in section 2. To check that the solution is not affected by the exterior damping, another experiment (not shown) was performed with a zonally uniform basic state (Greenwich section) but the same 3D damping structure. In this case the wave continues well past  $60^\circ\text{W}$ , unlike the true solution shown in Fig. 4. We are therefore satisfied that the zonal variations in the solution are a property of the AEJ and not the experimental design.

The wave grows with an  $e$ -folding time of 4 days. This growth rate lies between the two values for Greenwich-jet-maximum and sector-average basic states presented above. The vertical structure shows broadly the same surface intensified character as before, reflecting the strong vertical shear and low static stability at low levels, but there is also a clear downstream development even in this single coherent linear mode. At inception ( $30^\circ\text{E}$ ) the wave is confined to low levels. At the jet maximum ( $0^\circ$ ) there is a deeper structure and a two-way tilt against the shear above and below the jet core. As the wave weakens again ( $30^\circ\text{W}$ ) the peak lifts off the surface and moves into phase in the vertical. The phase speed therefore varies both with longitude and height to preserve this complex spatial structure at a single frequency.

When low-level damping is applied to momentum and temperature there are some visible changes in the

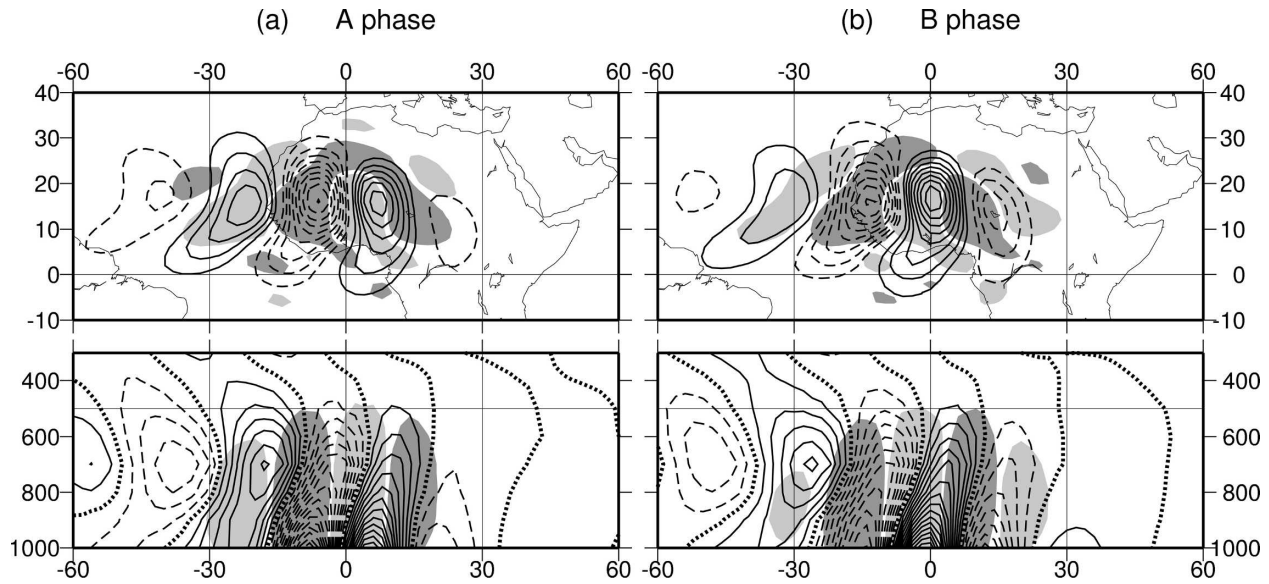


FIG. 5. As in Fig. 4 but for the modal structure that emerges when low-level damping is applied.

spatial characteristics of the mode. The result is shown in Fig. 5. The wave packet has effectively shifted westward. The surface-intensified section to the east is attenuated more than the rest of the wave, so there is a shorter lead-in to the wave maximum west of Greenwich. Furthermore, the upstream–downstream contrast in tilt and vertical structure is now accentuated. We see therefore that a preferential damping at low levels affects both the vertical and longitudinal distribution of wave amplitude in ways that are not apparent with zonally uniform experiments. The shifted mode now bears a very close resemblance to the observed regressions. Compare Fig. 5 with the composite structures shown in Fig. 3 of Part I. The A phase matches with their day 0 composite and the B phase falls around their day +1. The vertical structure here closely resembles the observed, with the strongest perturbations elevating to near the jet level as the wave propagates offshore (cf. Figs. 6 and 7 in Part I). The phase relationship between streamfunction and OLR is largely reproduced with vertical velocity in the adiabatic dynamical mode shown here. Near the jet maximum there is ascent in the northlies, but just downstream the ascent is in phase with the trough. This will be discussed further in section 5.

The other important consequence of damping the mode on the wavy basic state is that the growth rate has now become negative (see Table 2). The system is now just stable and decays slowly with time. Supplementary experiments show that once the damping has stabilized the system, it is relatively insensitive to any increase in the strength of the damping and remains close to neutral, similar to the behavior found by HS98.

Further information about the longitudinal structure of the mode can be diagnosed from eddy fluxes as before. The integrated effect of the wave at a given longitude must be calculated over one periodic cycle, discounting the effect of growth or decay of the mode, to give characteristic second-order moments (it can be shown that a simple average of the fluxes associated with the normalized A and B phases gives the same spatial structures). The fluxes are shown in Fig. 6 for three sector averages. The sectors are (from right to left)  $0^{\circ}$ – $30^{\circ}$ E,  $30^{\circ}$ W– $0^{\circ}$ , and  $60^{\circ}$ – $30^{\circ}$ W. These sectors are chosen to represent the initiation, maximum, and dissipative phases of the damped mode, respectively. The change in structure of momentum and temperature fluxes through the wave packet illustrates the progression from baroclinic to barotropic growth mechanisms anticipated from the structure of the mode. The fact that the mode is slowly decaying does not alter this basic signature. At inception and wave maximum, the southward temperature flux is very strong and surface intensified, but it weakens rapidly in the dissipation region to the west. Westward momentum flux is convergent everywhere, feeding the wave. It also weakens to the west, but not as dramatically as the temperature flux. In consequence the system can be viewed as more barotropic to the west. The fluxes associated with the dynamical mode again stand up to close comparison with the observed composites of Part I (cf. Fig. 6b with their Fig. 13).

These findings are confirmed by the energy conversion diagnostics, which have been calculated for the same three sectors and are shown in Table 2 for both

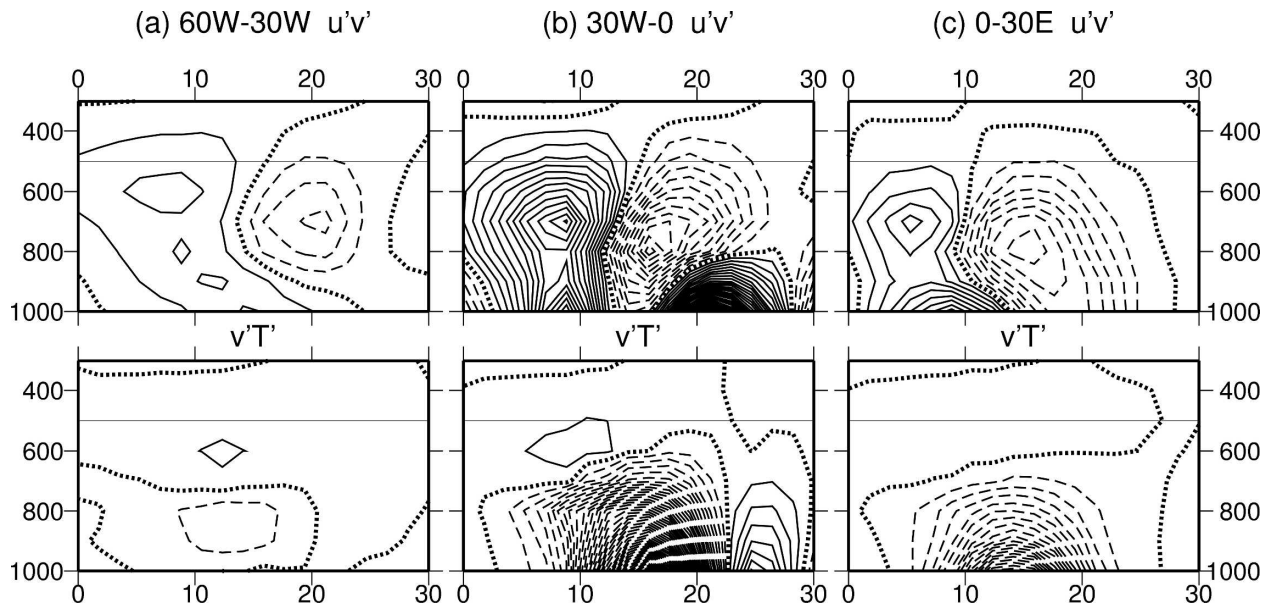


FIG. 6. Wave-wave components of northward fluxes of (top) westerly momentum and (bottom) temperature associated with damped normal mode on a wavy basic state in three different sectors: (a)  $60^{\circ}$ – $30^{\circ}$ W, (b)  $30^{\circ}$ W– $0^{\circ}$ , (c)  $0^{\circ}$ – $30^{\circ}$ E. Contour intervals are arbitrary but constant so magnitudes can be compared, zero contour dotted, negative contours dashed.

damped and undamped modes. Before discussing these numbers it must be stressed that for modes on a wavy basic state, they no longer represent a complete description of the processes assigned to them in the zonal mean energy budget for the system. This is because the basic state itself now has large departures from its zonal mean. The energy conversions are defined in terms of second-order moments of departures from the zonal mean. This leads to self-interaction terms for the basic state and interaction terms between the wave and the basic state. We might argue that the former is not a property of easterly waves, but the latter may be important, and it is impossible to calculate for a linear mode with arbitrary amplitude. The numbers given in Table 2 only represent the wave-wave interaction and therefore only serve as a quantitative guide to the wave structure and not as a statement of the energy budget. Nevertheless the picture is complicated. In terms of the ratio of baroclinic to barotropic conversions, the wavy basic-state modes are less baroclinic than the corresponding Greenwich section modes, and more baroclinic than the sector average mode. On the whole, for the wavy basic state, the modes turn out to be more baroclinic when damped. This occurs for the same reason as before with the modes growing on zonally uniform basic states: there is a relatively large reduction in low-level wave activity and its correlation with low-level meridional wind. For the same reason the contrast between the three sectors is much more marked for the damped mode on a wavy basic state: barotropic con-

versions are slightly stronger than baroclinic conversions in the west, and the wave is very baroclinic over the continent.

The AEJ has a seasonal cycle from June to September. The jet maximum is strong in June and weak in August, shifting west and north in July and east from July to September, as shown in Fig. 7. Separate experiments for each climatological monthly mean (1968–98) were carried out with and without damping. The results for the growth rate are given in Table 3. The growth rates for the undamped modes vary around the JJAS mean value, stronger in June and weaker in September. Low-level damping effectively neutralizes all the modes. The structures for one phase of the damped modes are shown alongside their respective basic states in Fig. 7. The modes basically follow the jet core and look very similar to the seasonal mean mode, except for September, which extends further to the east and has a curious double structure with maximum amplitude over the jet entrance and a break over West Africa. Note that in each case there is ascent in the northerlies under the jet core and in the trough downstream. Also shown in Fig. 7 and Table 3 are the results for two further basic states: July–August means from 1988 and 1990. These two periods were chosen based on tropical depression (TD)-filtered OLR diagnostics (as in Part I). The former, 1988, was a very active year for easterly waves. The latter, 1990, was a very quiet year. The contrast between the two years does not appear to be clearly linked with the mean state of the AEJ. It has a very

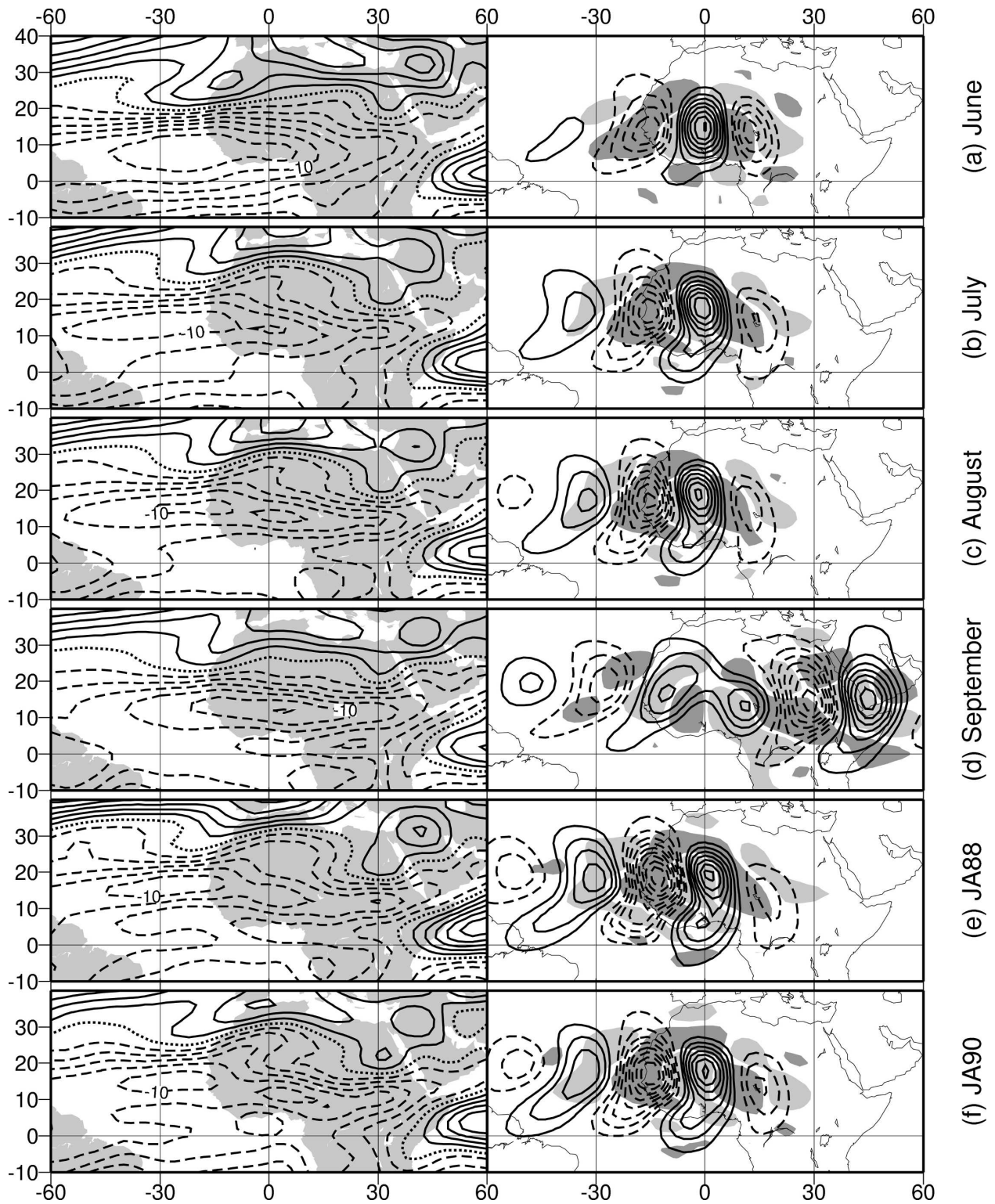


FIG. 7. (left) Zonal wind at  $\sigma = 0.65$  and (right) streamfunction and vertical motion at  $\sigma = 0.85$  for associated damped modal structure for various basic states: (a) Jun 1968–98, (b) Jul 1968–98, (c) Aug 1968–98, (d) Sep 1968–98, (e) Jul–Aug 1988, (f) Jul–Aug 1990. Contour intervals are  $2 \text{ m s}^{-1}$  for wind and arbitrary for streamfunction, zero contour dotted (omitted for streamfunction), negative contours dashed. Regions of ascent are heavily shaded and descent lightly shaded.

TABLE 3. Growth rates ( $\text{day}^{-1}$ ) of damped and undamped normal modes for wavy basic states based on the four individual summer months (JJAS) and associated with active (1988) and inactive (1990) easterly wave episodes.

Basic state	Undamped	Damped
Jun 1968–98	0.33	0.06
Jul 1968–98	0.25	0.03
Aug 1968–98	0.25	0.02
Sep 1968–98	0.20	−0.09
Jul–Aug 1988	0.17	−0.05
Jul–Aug 1990	0.23	−0.1

similar structure and magnitude and the associated modes are also similar. The 1990 undamped mode actually grows faster. With damping, both modes decay. The implications of this for understanding African easterly wave variability will be discussed in the next section.

## 5. Discussion

In this paper we have used reanalysis data to furnish realistic zonally uniform and wavy basic states and deduced normal mode structures for the African easterly jet. This is a development on previous work, which mostly relied on idealized zonally uniform basic states. The results are correspondingly more complicated, but show a close resemblance to the observed composites of AEWs presented in Part I.

One of the principal differences between our solutions and those of more idealized studies (e.g., TH94a) is their intensity near the surface. This is a result of having a stronger low-level vertical shear and low static stability, and weaker jet level horizontal shear. The baroclinic nature of the modes compared to idealized studies is also illustrated by the energy conversion diagnostics, particularly in the upstream region. This is in accord with recent realistic limited area modeling work by Hsieh and Cook (2005, 2006), who find that easterly waves can be generated without recourse to barotropic instability of the AEJ, although in their studies convective heating within the wave plays an important role.

Like TH94a, we have low-level ascent in the northerlies for our zonally uniform basic states and near the strongest part of the jet over the continent for our wavy basic states. The vertical motion is consistent with the vertical gradient of vorticity advection by the basic-state zonal flow. This is true in spite of the surface-intensified nature of the vorticity perturbation, because of the strength of the basic-state shear: at low levels we actually have westerlies. Indeed, zonal variations not only in the AEJ but also in the lower-level westerlies contribute to the changing baroclinic–barotropic nature

of the waves as they propagate westward. The associated vorticity advection is illustrated in Fig. 8a, which shows the zonal wind, and the phase relationship between perturbation vorticity and vertical motion at  $15^\circ\text{N}$ , for the damped JJAS experiment on a wavy basic state (for a phase that falls between  $-A$  and  $-B$  as defined above). The vorticity, and hence vorticity advection, remains in a constant phase relationship with the vertical motion, with increasing positive perturbation vorticity advection by the mean wind with height. This gives rise to upward motion at low levels where the basic-state vertical shear is strong, and weakens around  $30^\circ\text{W}$  as the shear collapses. Figure 8b shows the integral of this vorticity perturbation: the meridional wind. Upward motion is clearly in the northerlies around Greenwich but the phase relationship drifts somewhat as we integrate the decaying vorticity signature westward. Integrating again, Fig. 8c shows the relationship with streamfunction and here we see upward motion located in the trough at  $30^\circ\text{W}$ . The apparent variable phase relationship of the vertical motion with the wave can thus be understood as a consequence of dynamical balances in a wave packet that decays westward in amplitude. To further illustrate the dynamical origin of the vertical motion, and by implication deep convection, we repeat here the  $\mathbf{Q}$  vector analysis presented in Part I. The definition of  $\mathbf{Q}$  in terms of rotational winds is given in their Eqs. (1) and (2), and can be summarized as

$$\mathbf{Q} = (Q_1, Q_2) = -\frac{R}{p} \left( \frac{\partial \mathbf{v}_\psi}{\partial x}, \frac{\partial \mathbf{v}_\psi}{\partial y} \right) \cdot \nabla T,$$

where  $\mathbf{v}_\psi$  is the horizontal nondivergent velocity vector. In Fig. 9a  $\mathbf{Q}$  is plotted for our dynamical modes. As with the energy diagnostics presented above, we note that for a modal perturbation of undefined amplitude it is meaningless to present the sum of all the interaction terms, and here we concentrate on the wave–mean flow terms that are dominant when considering phase relationships (as opposed to zonally integrated quantities). Convergence of  $\mathbf{Q}$  represents an adiabatic source term on the right-hand side of the omega equation and is calculated for the nondivergent flow according to

$$\left( \frac{p}{R} \right) \nabla \cdot \mathbf{Q} = J(T, \xi) + \psi_{xy}(T_{xx} - T_{yy}) - T_{xy}(\psi_{xx} - \psi_{yy}), \quad (6)$$

where  $J$  is the Jacobian and subscripts denote derivatives [cf. Eq. (A3) in Part I]. The first term in (6) dominates the solution and can be thought of as the advection of vorticity by the thermal wind. As in Part I the mean flow advection part  $J(\bar{T}, \xi')$  accounts for most of the signal. Convergent  $\mathbf{Q}$  vectors coincide neatly with

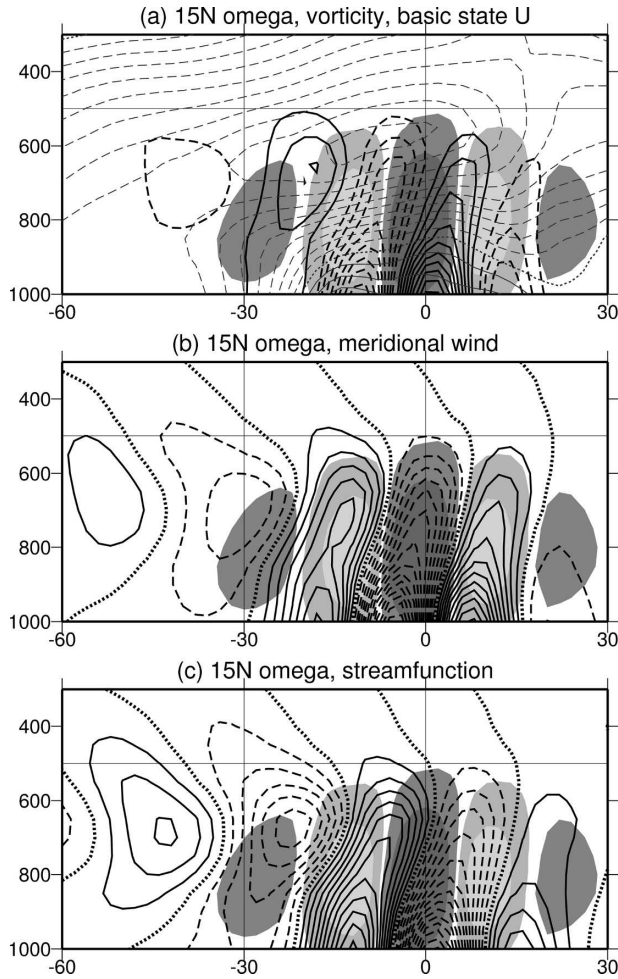


FIG. 8. Phase relationships at 15°N between vertical motion and other dynamical fields for the damped mode at a position 60% of the way from  $-A$  to  $-B$  in the cycle. Two-tone shading on all plots is ascent (heavy) and descent (light). (a) Perturbation vorticity (heavy contours) and basic state zonal wind (light contours,  $1 \text{ m s}^{-1}$ ), (b) perturbation meridional wind, (c) perturbation streamfunction. Negative contours dashed. Zero contour dotted, or omitted for vorticity perturbations.

ascent in the strongest part of the wave and there is some similarity with the situation at lag  $-1$  day in the composites of Part I (their Fig. 14b). The resemblance of the adiabatic dynamical modes studied here to the composites for streamfunction and OLR shown in Part I is possibly fortuitous but certainly suggestive, and bears further investigation. Miller and Lindzen (1992) have shown that the low-level ascent generated by an unstable easterly jet can be sensitive to the nature of the shear below the jet. How do their conclusions carry over to a longitudinally varying jet and to what extent does dynamically generated vertical motion govern convection in real easterly waves? Further modeling studies are needed to address this question.

A more fundamental question is to what extent normal modes can actually represent easterly waves at all. Is a pure shape-preserving structure the best way to understand a wave phenomenon that often exists for no longer than its own oscillation period and is sometimes difficult to distinguish from isolated traveling vorticity centers? The answer depends on whether one is just trying to describe the structure and dynamical mechanisms associated with easterly waves or whether one is seeking a theory for their origin. The damped modes shown in this study look realistic. Their longitudinal variation, and the way they draw energy from the mean flow is reminiscent of observed composites. But they are not unstable. A reasonable amount of low-level damping reduces the growth rates to near neutral. Many of the studies that have focused on growth rates or potential vorticity gradients appear to follow the hypothesis that if an instability is established, the natural variability of the AEJ will provide the origin of the waves, presumably at times of maximum instability. The potential vorticity (PV) gradient reversals are generated by radiative convective forcing (Schubert et al. 1991) and eroded by the waves. A thorough analysis of this process in a limited area model has recently been provided by J.-S. Hsieh and K. H. Cook (2005, personal communication). However well verified this mechanism may be, it does not necessarily provide a complete theory for the intermittence of AEWs. In this regard, our comparison of the contrasting years 1988 with 1990 is an instructive failure. The resulting structures were very similar and with damping they were both close to neutral. The AEJ will not generate these wave structures from any small random perturbation. A big perturbation is needed. Given a finite-amplitude perturbation upstream, structures resembling these normal modes will emerge, and this is the subject of our next contribution. These are the structures that are best able to maintain themselves against dissipation, and are therefore expected to outlast the initial perturbation, whatever it might be. It is not necessary that they conform exactly to the normal mode structures produced here, and some nonmodal structures might be more efficient for a limited time, but the basic structure of the fluxes and the energy conversions are likely to be similar. So if the system is near to neutral at all times, this suggests that the abundance of easterly waves in 1988 stems from an abundance of initial perturbations, rather than a difference in the mean jet. Instability may play a role for more limited times if the shear below the jet becomes particularly strong, and this possibility has not been fully refuted in this paper. The relevance of the instability hypothesis that previous idealized studies rely upon depends on whether the jet can get strong

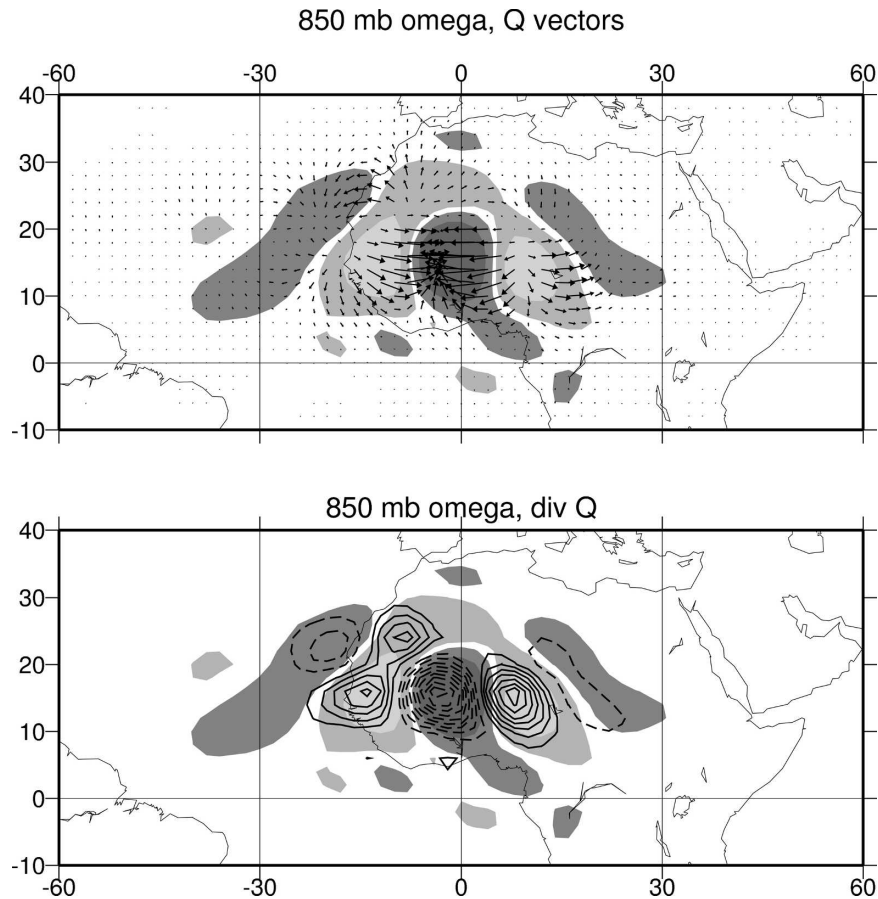


FIG. 9. The 850-mb vertical motion and forcing of vertical motion for the same phase as shown in Fig. 8. Two-tone shading on both plots is ascent (heavy) and descent (light). (a) Wave-mean flow  $\mathbf{Q}$  vectors. (b) Divergence of  $\mathbf{Q}$  vectors. Contour intervals and vector scale are arbitrary, negative contours dashed, zero contour omitted.

enough for long enough. This is by no means obvious, and will be the subject of future research. On the other hand the hypothesis that upstream triggering is of importance is borne out by a recent analysis of precursor events by Mekonnen et al. (2006). A striking example of an initial perturbation in convection giving rise to a wave structure and subsequently a hurricane is also described by Berry and Thorncroft (2005).

## 6. Conclusions

The work presented here can be summarized in terms of the following specific conclusions:

- 1) Taking account of the jet entrance–exit structure of the AEJ in a dynamical modeling study leads to longitudinal variations in the wave structure that resemble observed composites. The waves are baroclinic and grow closer to the surface upstream and become more barotropic downstream. These varia-

tions are seen in the linear normal modes of a climatological basic state. Although they may be important in real AEWs, nonlinear processes and the influence of diabatic heating in the wave are not included in this study. Nevertheless, the three-dimensional basic state alone leads to dynamical solutions that reproduce many of the observed upstream–downstream characteristics of AEWs. One of these characteristics is the dynamically balanced vertical velocity of the mode. This displays the same variable phase relationship with streamfunction as is seen for negative OLR (enhanced convection) anomalies in the observed composites of Part I. This suggests a link between the large-scale dynamics of the waves and the organization of convection, although the mechanism has yet to be elucidated.

- 2) The presence of surface westerlies, and of a zonal mean meridional circulation both lead to important modifications of the dynamical modes compared to

previous more idealized studies. A weaker jet with strong low-level shear and weaker static stability favors more baroclinic, surface-intensified systems. However, barotropic conversions between zonal and eddy kinetic energy also change significantly through the introduction of terms involving the meridional flow.

- 3) Although the basic state is dynamically unstable, the inclusion of a relatively modest amount of low-level damping can easily stabilize the system. This brings a new perspective to the classical hypothesis that easterly waves are generated by an instability mechanism, and prompts us to seek alternative mechanisms for their generation.

Further work is needed to resolve the questions discussed above pertaining to the origin and intermittency of AEWs. Finite-amplitude perturbations that can initiate the waves need to be identified and the temporal relationship between easterly waves and the state of the AEJ needs to be established. Since the waves extract energy from the jet it is natural to expect some relationship. However, our findings in this paper suggest that a complete theory for the intermittency of AEWs will also involve finite-amplitude precursors. The generation of AEWs will be the subject of our next contribution.

*Acknowledgments.* We thank the three anonymous reviewers for suggestions and criticisms that have led to improvements in the manuscript. NMJH was supported by the CNRS. GNK was supported by NOAA's Office of Global Programs under Grant GC01-351. CDT was supported by NSF Grant ATM 0138290.

#### REFERENCES

- Berry, G. J., and C. D. Thorncroft, 2005: Case study of an intense African easterly wave. *Mon. Wea. Rev.*, **133**, 752–766.
- Burpee, R. W., 1972: The origin and structure of easterly waves in the lower troposphere of North Africa. *J. Atmos. Sci.*, **29**, 77–90.
- Céron, J.-P., and J.-F. Guérémy, 1999: Validation of the space–time variability of African easterly waves simulated by the CNRM GCM. *J. Climate*, **12**, 2831–2855.
- Chang, C.-B., 1993: Impact of desert environment on the genesis of African wave disturbances. *J. Atmos. Sci.*, **50**, 2137–2145.
- Charney, J. G., and M. E. Stern, 1962: On the stability of internal baroclinic jets in a rotating atmosphere. *J. Atmos. Sci.*, **19**, 159–172.
- Dickinson, M., and J. Molinari, 2000: Climatology of sign reversals of the meridional potential vorticity gradient over Africa and Australia. *Mon. Wea. Rev.*, **128**, 3890–3900.
- Fjortoft, R., 1950: Application of integral theorems in deriving criteria for stability for laminar flows and for the baroclinic circular vortex. *Geophys. Publ.*, **17**, 1–52.
- Fyfe, J. C., 1999: Climate simulations of African easterly waves. *J. Climate*, **12**, 1747–1769.
- Grist, J. P., S. E. Nicholson, and A. I. Barcilon, 2002: Easterly waves over Africa. Part II: Observed and modeled contrasts between wet and dry years. *Mon. Wea. Rev.*, **130**, 212–225.
- Hall, N. M. J., 2000: A simple GCM based on dry dynamics and constant forcing. *J. Atmos. Sci.*, **57**, 1557–1572.
- , and P. D. Sardeshmukh, 1998: Is the time–mean Northern Hemisphere flow baroclinically unstable? *J. Atmos. Sci.*, **55**, 41–56.
- Hsieh, J.-S., and K. H. Cook, 2005: Generation of African easterly wave disturbances: Relationship to the African easterly jet. *Mon. Wea. Rev.*, **133**, 1311–1327.
- , and —, 2006: On the energetics of African easterly waves. *J. Atmos. Sci.*, in press.
- Kalnay, E., and Coauthors, 1996: The NCEP/NCAR 40-Year Reanalysis Project. *Bull. Amer. Meteor. Soc.*, **77**, 437–471.
- Kiladis, G. N., C. D. Thorncroft, and N. M. J. Hall, 2006: Three-dimensional structure and dynamics of African easterly waves. Part I: Observations. *J. Atmos. Sci.*, **63**, 2212–2230.
- Kwon, H. J., 1989: A reexamination of the genesis of African waves. *J. Atmos. Sci.*, **46**, 277–292.
- Mass, C., 1979: A linear primitive equation model of African wave disturbances. *J. Atmos. Sci.*, **36**, 2075–2092.
- Mekonnen, A., C. D. Thorncroft, and A. Aiyer, 2006: Analysis of convection and its association with African easterly waves. *J. Climate*, in press.
- Miller, R. L., and R. S. Lindzen, 1992: Organization of rainfall by an unstable jet with an application to African waves. *J. Atmos. Sci.*, **49**, 1523–1540.
- Norquist, D. C., E. E. Recker, and R. J. Reed, 1977: The energetics of African wave disturbances as observed during phase III of GATE. *Mon. Wea. Rev.*, **105**, 334–342.
- Paradis, D., J.-P. Lafore, J.-L. Redelsperger, and V. Balaji, 1995: African easterly waves and convection. Part I: Linear simulations. *J. Atmos. Sci.*, **52**, 1657–1679.
- Reed, R. J., D. C. Norquist, and E. E. Recker, 1977: The structure and properties of African wave disturbances as observed during Phase III of GATE. *Mon. Wea. Rev.*, **105**, 317–333.
- Rennick, M. A., 1976: The generation of African waves. *J. Atmos. Sci.*, **33**, 1955–1969.
- Schubert, W. H., P. E. Ciesielski, D. E. Stevens, and H.-C. Kuo, 1991: Potential vorticity modeling of the ITCZ and the Hadley circulation. *J. Atmos. Sci.*, **48**, 1493–1509.
- Simmons, A. J., 1977: A note on the instability of the African easterly jet. *J. Atmos. Sci.*, **34**, 1670–1674.
- Thorncroft, C. D., 1995: An idealised study of African easterly waves. III: More realistic basic states. *Quart. J. Roy. Meteor. Soc.*, **121**, 1589–1614.
- , and B. J. Hoskins, 1994a: An idealised study of African easterly waves. I: A linear view. *Quart. J. Roy. Meteor. Soc.*, **120**, 953–982.
- , and —, 1994b: An idealised study of African easterly waves. II: A nonlinear view. *Quart. J. Roy. Meteor. Soc.*, **120**, 983–1015.